Supporting Information

Multifunctional ionic liquid additive providing solvation structure and electrostatic shielding layer for high-stable aqueous zinc ion batteries

1. Experimental section

Electrolyte preparation: Zinc sulfate ($ZnSO_4$, Macklin, 99%) was dissolved in deionized (DI) water to prepare a 2 M $ZnSO_4$ electrolyte, which was used as a blank electrolyte(BE). The control group used different concentrations (0.5%, 1%, 1.5%) of 1-butyl-3-methylimidazolium hexafluorophosphate ($C_8H_{15}F_6N_2P$, Aladdin, 99%, [BMIM]PF_6) was added to the prepared 2 M $ZnSO_4$ electrolyte to obtain the [BMIM]PF_6 additive-containing .The optimum concentration of [BMIM]PF_6 systems is 1% [BMIM]PF_6 + 2 M $ZnSO_4$, and the corresponding electrolyte is abbreviated as [BMIM]PF_6/BE.

Preparation of electrodes Purchased zinc foils (thickness: 100 μm, 99.99%) were polished with sandpaper to remove the passivation layer. The Zn foil was then cut into a disc with a diameter of 16 mm to serve as the Zn electrode. $NH_4V_4O_{10}$ was synthesized using a hydrothermal method. i.e. 1.17 g of ammonium vanadate (NH_4VO_3, Aladdin, AR) was dissolved in 70 mL of deionized water. Then 1.891 g of oxalic acid (Aladdin, AR) powder was added to the NH_4VO_3 solution under magnetic stirring. The solution was transferred to a 100 mL tetrafluoroethylene lined autoclave and heated at 140 °C for 12 h. After cooling, the product was collected, washed repeatedly with deionized water, and then dried at 70 °C overnight to give the final $NH_4V_4O_{10}$ powder. A $NH_4V_4O_{10}$ electrode slurry was formed by fusion stirring with $NH_4V_4O_{10}$ powder, Ketjen black (KB), and PTFE (mass ratio 75:15:10), and then the slurry was cast on a stainless steel mesh. After drying in air at 70 °C overnight, $NH_4V_4O_{10}$ electrodes containing 1.3-2.6 mg cm^{-2} were finally obtained.

The monomer (2 g acrylamide) was dissolved in 10mL of an aqueous electrolyte (2 M $ZnSO_4$), and then the initiator [15 mg $(NH_4)_2S_2O_8$ (Aladdin, AR)] and cross-linking agent [2.5 mg N, N'-methylene bis(acrylamide) (Aladdin, 99%)] were added and stirred for 30 min. Alternatively, it was injected into a mold of the designed

thickness. After polymerization at 60 °C for 1.5 h, a Polyacrylamide (PAM) hydrogel film was formed, named PAM. the composite gel electrolyte obtained by adding 1% [BMIM]PF_6 before polymerization was noted as PAM-1%[BMIM]PF_6.

2.Test section

Materials Characterization: The prepared NH_4VO_3 powder and zinc anode were physically analyzed using a MiniFlex600 X-ray diffractometer. The XRD scanning range used in the experiments was 5~80°, and the XRD scanning speed was set at 10°/min. Fourier transform infrared (FTIR) spectroscopy was tested by a Nicolet IS10 Fourier transform infrared spectrometer, with a scanning range of 4000 cm^{-1}~400 cm^{-1}. X-ray photoelectron spectroscopy was collected by an EscaLab Xi^+ XPS system. X-ray photoelectron spectra were collected by the EscaLab Xi^+ XPS system, which uses a monochromatic Al Kα X-ray source (*hv* = 1486.6 eV). The morphology of the samples was observed by a field emission scanning electron microscope (SEM, Gemini SEM 300) field emission scanning electron microscope on the morphological structure of the experimental samples.

Electrochemical Characterization: Purchased zinc foils (thickness: 100 μm and 20 μm, 99.99%) were polished with sandpaper to remove the passivation layer. The zinc foil was then cut into a 16 mm diameter disc to serve as the zinc electrode. All tested CR2032 type coin batteries were assembled in an open-air environment using glass fiber filters (GF/D, Whatman) as diaphragms. The amount of electrolyte used for the coin battery was 120 μL. two identical zinc plates with a thickness of 100 μm were used to make a symmetrical battery. Zn//Cu half batteries were assembled using a copper foil of 20 μm thickness as the working electrode and a zinc foil of 100 μm thickness as the reference and counter electrodes. The $NH_4V_4O_{10}$//Zn full battery was assembled using a Zn plate with a thickness of 100 μm as the anode and $NH_4V_4O_{10}$ as the cathode. The blank electrolyte and [BMIM]PF_6 electrolyte were used for the electrolyte. The $NH_4V_4O_{10}$ cathode (16 mm

diameter, circular piece) was combined with the Zn anode (100 μm thickness), and glass fiber was used as the diaphragm to assemble the $NH_4V_4O_{10}$//Zn full battery. The $NH_4V_4O_{10}$ cathode (2 cm^2) was combined with a Zn anode (100 μm thickness) and assembled into $NH_4V_4O_{10}$//Zn flexible batteries using PAM-[BMIM]PF_6 hydrogel electrolyte as a flexible diaphragm. The $NH_4V_4O_{10}$//Zn battery was discharged/charged under a potential control of 0.3 ~ 1.4 V using a NEWARE battery tester.

Electrochemical characterization: Tafel plots were measured with Zn plate as the working electrode, Pt foil as the counter electrode, and saturated dimercury dichloride as the reference electrode, scanning at -0.7 ~ -1.2 V in 2 mV s^{-1} band. Chronoamperometry (CA), when measured at a fixed overpotential of -0.15 V. Cyclic voltammetry (CV) curves of plated/stripped zinc, were measured with a Zn//Ti battery in the voltage range of -1.5 V ~ 2.0 V at 1 mV s^{-1}. Hydrogen precipitation potentials were determined using linear scanning voltammetry (LSV) with a scan rate of 1 mV s^{-1} in the BE and [BMIM]PF_6/BE systems. The electrochemical impedance spectroscopy (EIS) of the Zn//Zn symmetric battery was analyzed in the frequency range of 0.01 Hz ~ 100 k Hz. By fitting the obtained R_{ct}, the activation energy E_a was calculated according to Arrhenius' law.

DFT calculation method:

The density functional theory (DFT) simulations are performed using the CASTEP program package in Materials Studio. The exchange-correlation interaction is described by generalized, gradient approximation (GGA) with the Perdew-Burke-Ernzerhof (PBE) functional.

For the construction of surface models, a 15 Å vacuum is used to eliminate interactions between periodic structures. And the Zn (002) slab is constructed with lattice constants of a = b = 15.6862 Å, c = 22.3097 Å, α = β = 90° and γ = 120°. And one molecular of $[BMIM]^+$ or H_2O is put on the Zn (002) surface. And the adsorption energy (E_{abs}) of $[BMIM]^+$ or H_2O on Zn (002) surface was calculated, by the formula: $E_{abs} = E_{total} - E_M - E_S$, where E_{total}, E_M and E_S are the energy of, respectively, the total system, the $[BMIM]^+$ or H_2O

molecular, and Zn (002) surface.

The binding energy ($E_{binding}$) between Zn^{2+}, $[BMIM]^{+}$,SO_4^{2-} and H_2O molecular was calculated by the, formula: $E_{binding} = E_{total} - E_a - E_b$, where E_{total} is the energy of the total system, E_a and E_b are the, energies of components in the system.

Molecular dynamic (MD) simulations

Molecular dynamic (MD) simulations were applied to investigate the solvation structures for two considered electrolytes denoted as S1 and S2. For S1 system, the solution was comprised of 50 $ZnSO_4$ and 1375 H_2O molecules. For S2, the solution contained 50 $ZnSO_4$, 10 $[BMIM]PF_6$ and 1375 H_2O molecules. All solution components were randomly packed into cubic simulation boxes. All MD simulations were carried out by Forcite module with COMPASS III force field [1, 2] in MS 2020. Van der Waals and Coulomb interactions were respectively considered by atom based and Ewald methods with a cut-off value of 12.5 Å. Equations of motion were integrated with a time step of 1 fs. After energy minimization, the electrolyte system was fully relaxed under periodic boundary conditions for 400 ps in the NPT (P = 1 atmosphere, T = 298.0 K) ensemble using the Nose thermostat and Berendsen barostat, which was long enough for system temperature, potential and total energy to get stable. After reaching equilibrium state, another 400 ps simulation under NVT ensemble was performed to extract trajectory and data for radical distribution function (RDF) and coordination number (CN) calculation. The dynamic trajectory for each system was outputted at an interval of 4 ps. The coordination number Ni of atom i in the first solvation shell surrounding Zn^{2+} was calculated as:

$$N_i = 4\pi\rho\int_0^{R_M} g\,(r) r^2 dr \quad (1)$$

in which R_M is the distance of the first minimum following the first peak in the RDF g(r) and ρ is the number density of atom i[3].

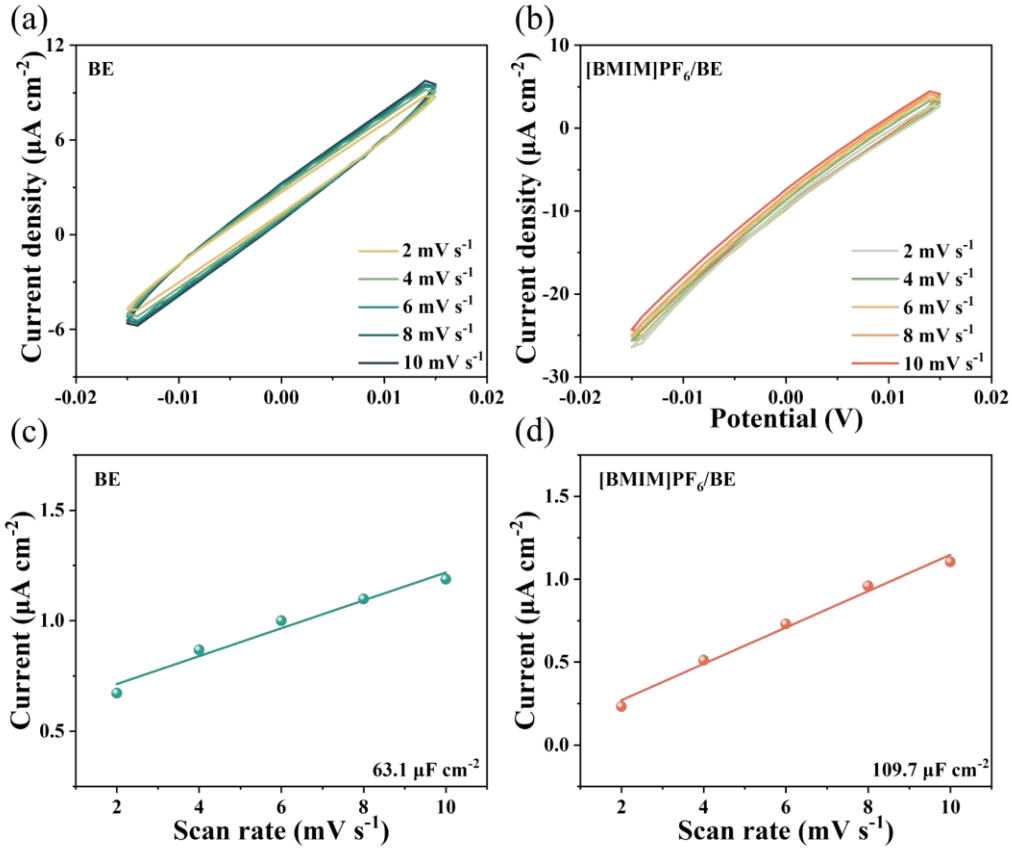

Fig. S1 The cyclic voltammetry (CV) curves for Zn//Zn cells in **(a)** BE system, **(b)** [BMIM]PF_6/BE system. The calculated electric double layer capacitance for cells in **(c)** BE system, **(d)** [BMIM]PF_6/BE system.

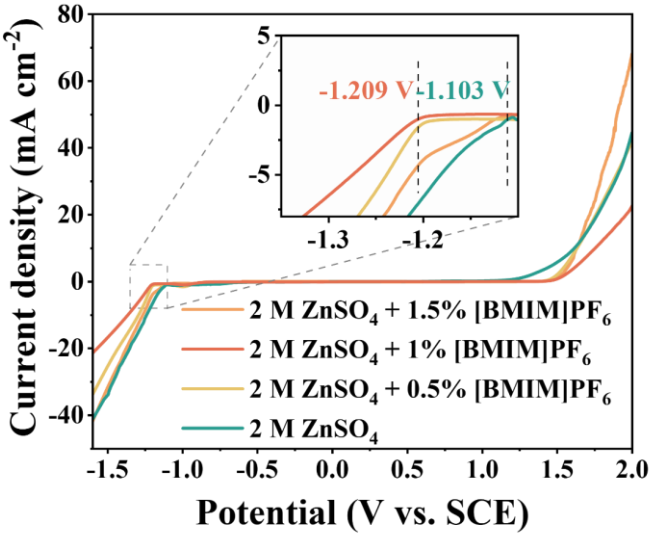

Fig. S2. The electrochemical stability window of the electrolytes with various doping concentrations of [BMIM]PF_6 additives was tested on Ti electrodes by scanning at a rate of 1 mV s^{-1}.

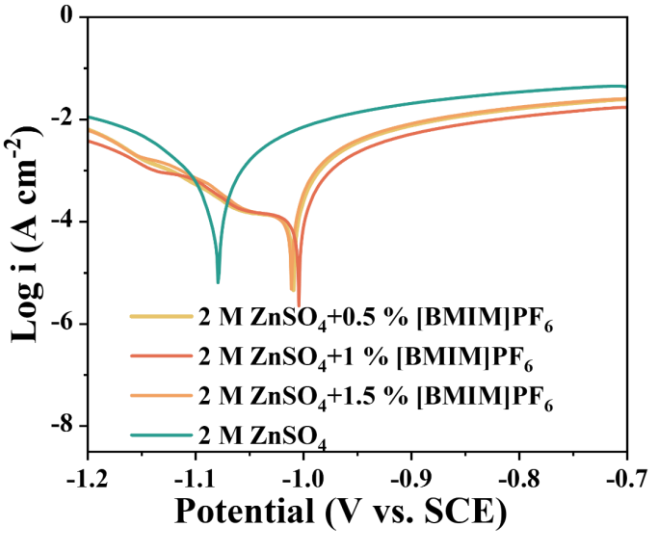

Fig. S3. Tafel curves for BE system and different concentrations of [BMIM]PF_6/BE systems.

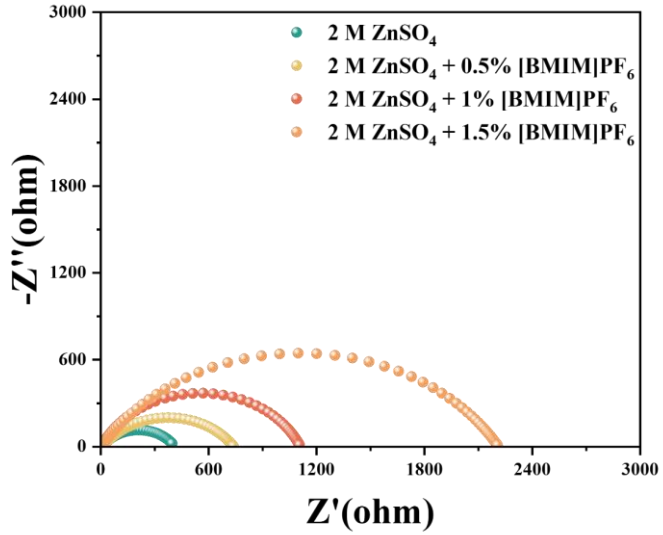

Fig. S4. Electrochemical impedance spectroscopy of batteries assembled with [BMIM]PF_6 at different concentrations.

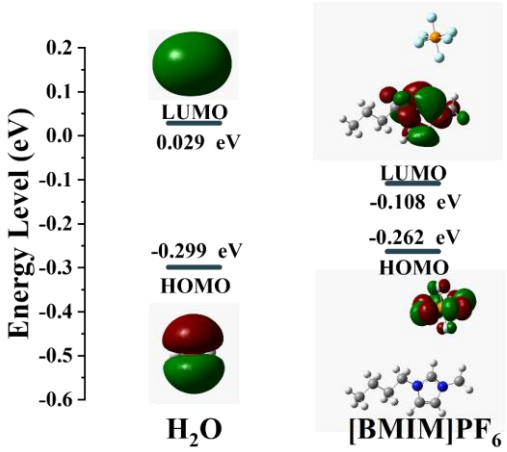

Fig. S5. LUMO, HOMO energy of H_2O molecules (**left**) and [BMIM]PF_6 (**right**).

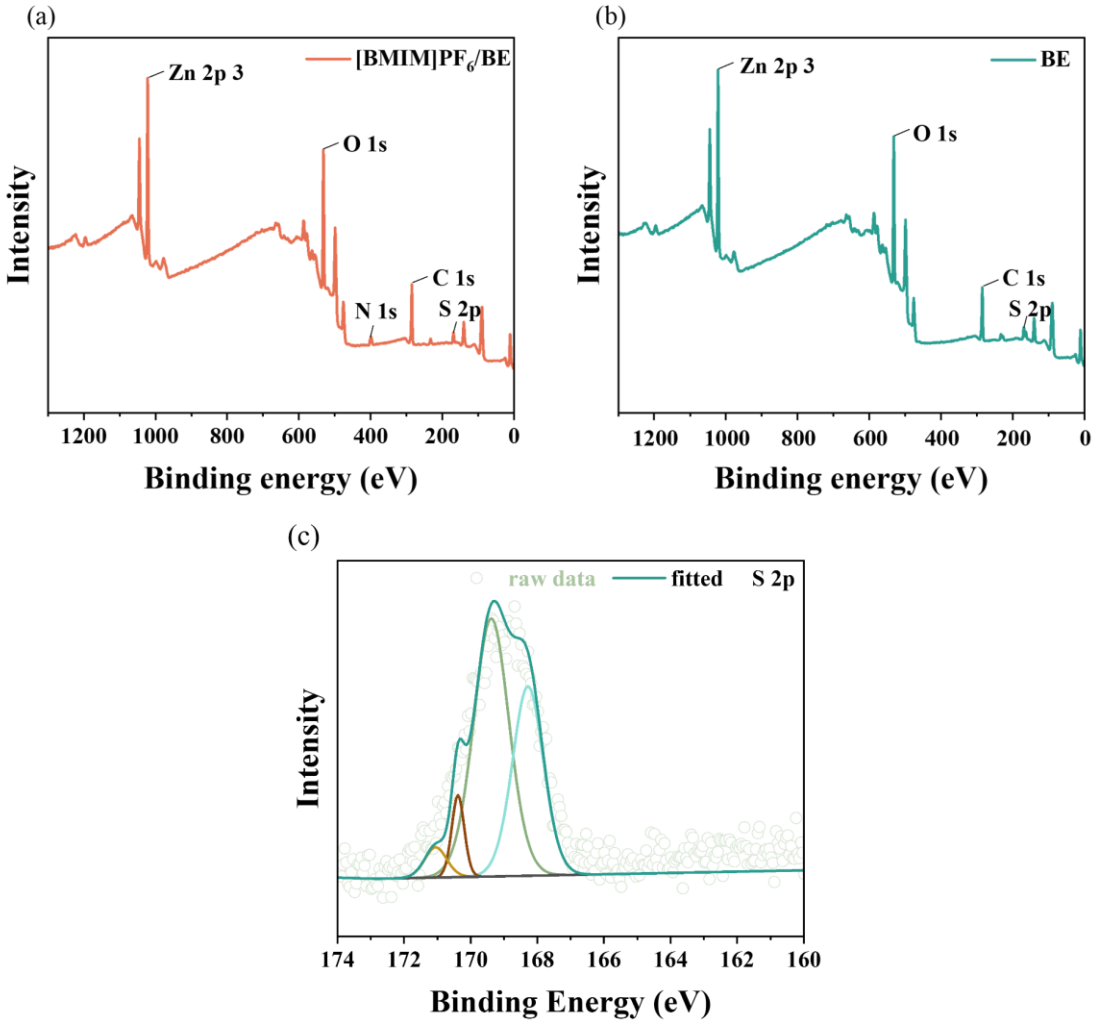

Fig. S6. High resolution XPS spectra of zinc metal electrodes after 50 cycles with **(a)** [BMIM]PF_6/BE system and **(b)** BE system at 1 mA cm^{-2} and 1 mAh cm^{-2}. High-resolution XPS spectra of the Zn metal electrodes after 50 cycles with BE system at 1 mA cm^{-2} and 1 mAh cm^{-2}: **(c)** S 2p.

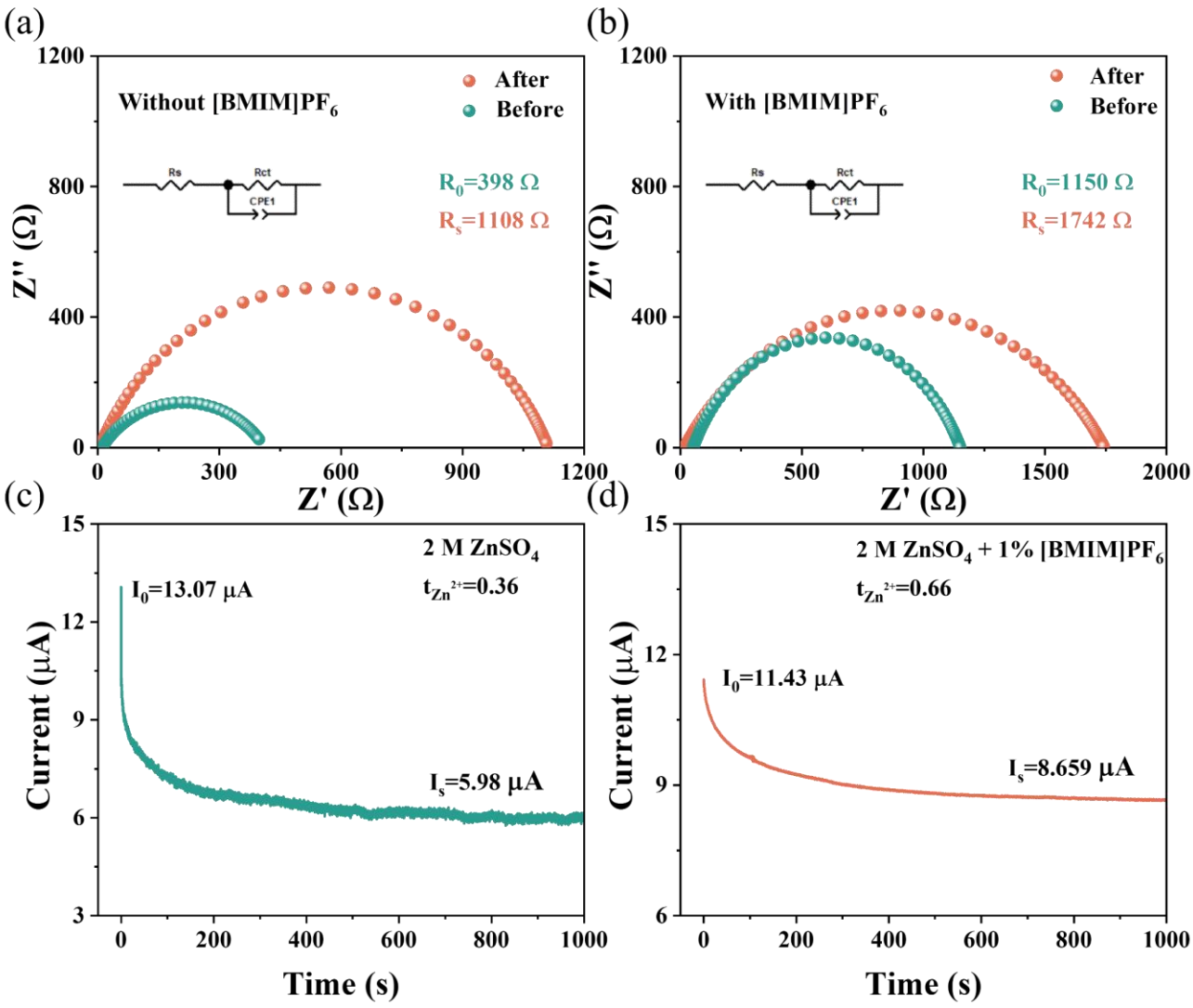

Fig. S7. Comparison of EIS curves of Zn//Zn symmetric cells in different electrolytes **(a)** initial and **(b)** after i-t test; current-time plots of electrolytes **(c)** without [BMIM]PF_6 and **(d)** with [BMIM]PF_6, respectively, at a constant voltage of 15 mV for 1000 seconds.

Auxiliary note: The Zn^{2+} transfer number (t_{zn}^{2+}) was calculated according to the BruceVincent method:

$$t_{zn^{2+}} = \frac{I_s(V - I_0R_0)}{I_0(V - I_SR_S)}$$

where V is the applied potential (15 mV); I_0 and R_0 are the initial current and the interface resistance; I_s and R_s represent the steady-state current and interface resistance, respectively. Therefore, the value of t_{zn}^{2+} can be calculated to be 0.66 for the [BMIM]PF_6/BE system, while the value is only 0.36 for the BE system.

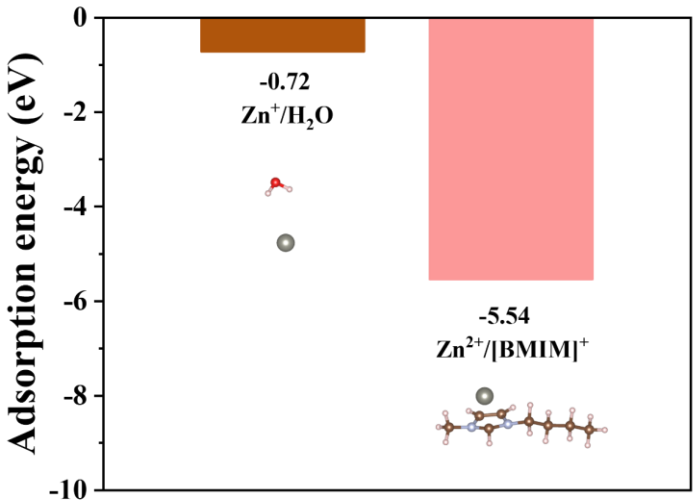

119

120 **Fig. S8.** The comparison of binding energies between Zn^{2+}&H_2O, Zn^{2+}&$[BMIM]^+$ and $[BMIM]^+$&H_2O.

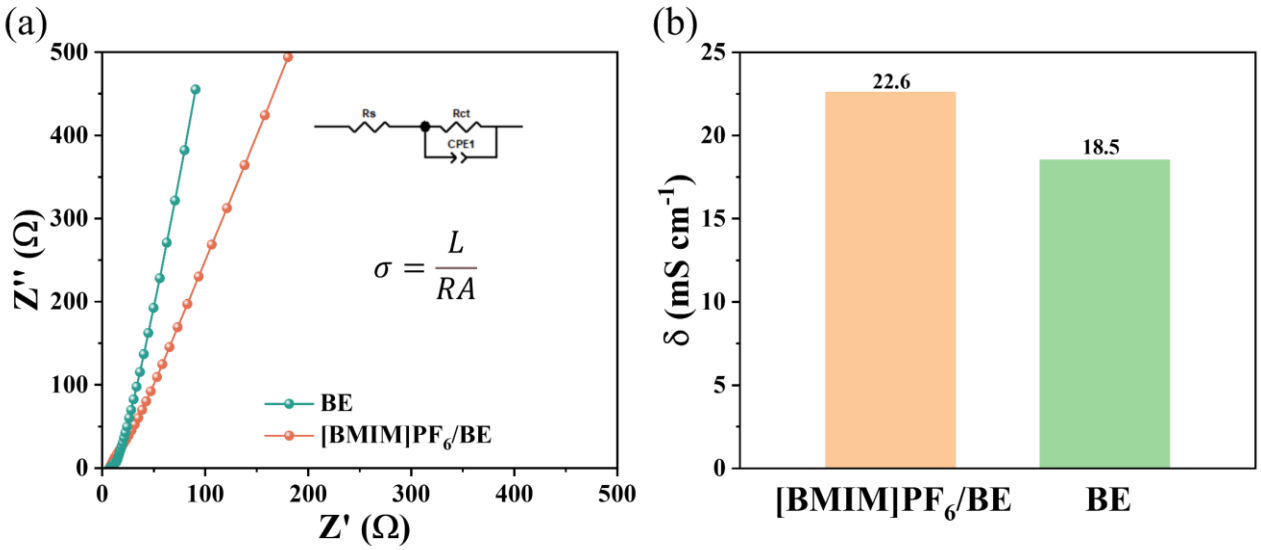

121

122 **Fig. S9. (a)** Impedance spectra and **(b)** ionic conductivities in the BE and $[BMIM]PF_6$/BE systems.

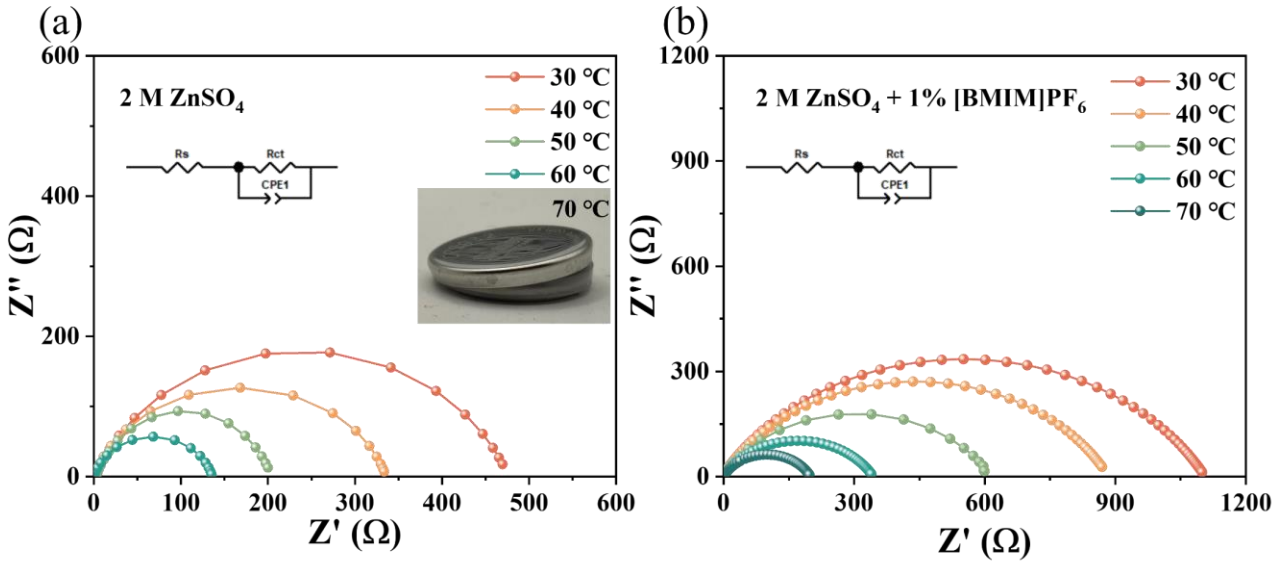

123

124 **Fig. S10.** Nyquist plots of Zn//Zn symmetric cells at different temperatures in **(a)** BE and **(b)**

125 [BMIM]PF_6/BE systems.

126

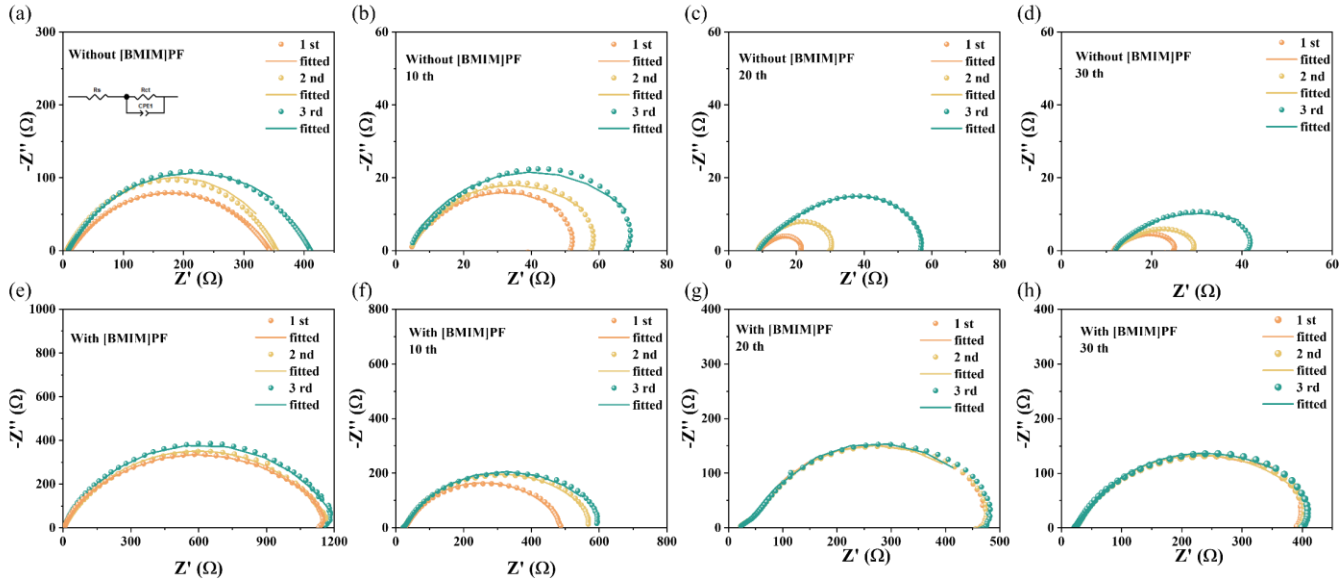

127

128 **Fig. S11.** Nyquist plots and fitted curves in the BE system without [BMIM]PF_6 **(upper panel)** and with

129 [BMIM]PF_6 **(lower panel)** at **(a)**, **(e)** 0 cycling cycle, **(b)**, **(f)** 10 cycling cycles, **(c)**, **(g)** 20 cycling cycles,

130 **(d)**, **(h)** 30 cycling cycles (three tests at the same cycle are shown in the same figure).

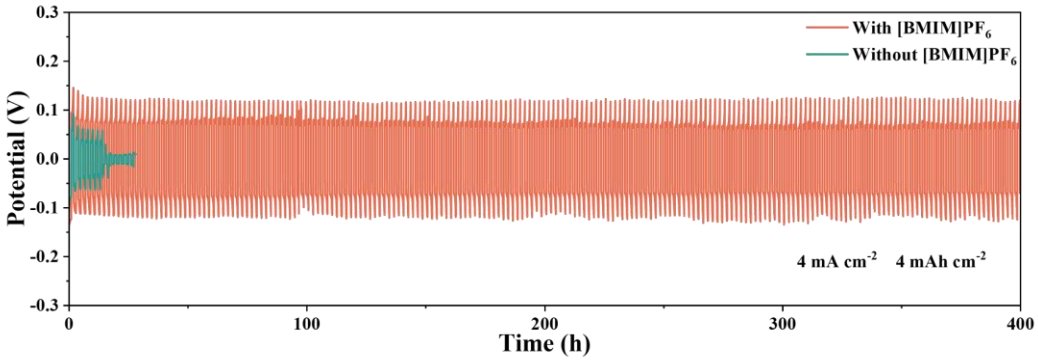

Fig. S12. Stability of Zn//Zn cells using electrolytes with [BMIM]PF_6 and without [BMIM]PF_6 additive at 4 mA cm^{-2} conditions.

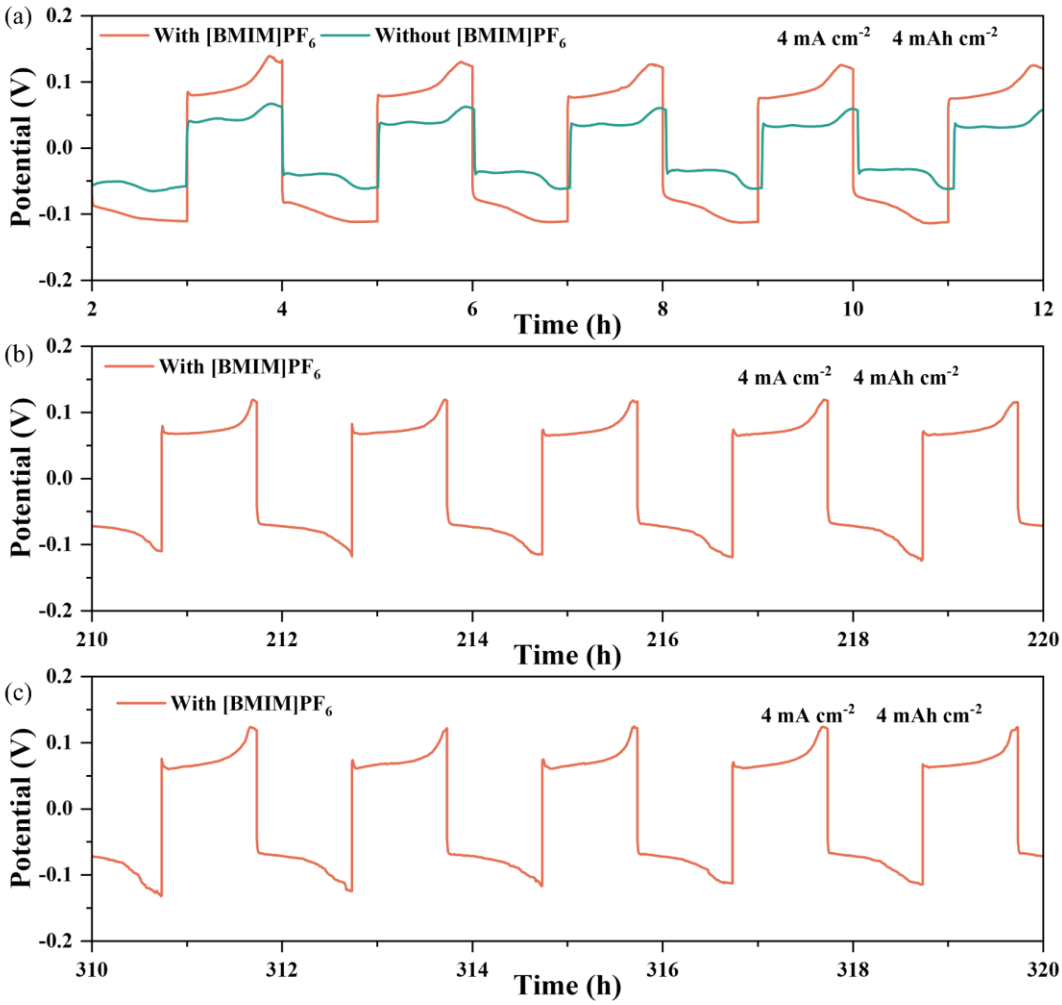

Fig. S13. Cycling stability of Zn//Zn batteries with and without [BMIM]PF_6 electrolytes under 4 mA cm^{-2}: **(a)** 10-20h; **(b)** 210-220h; **(c)** 310-320h.

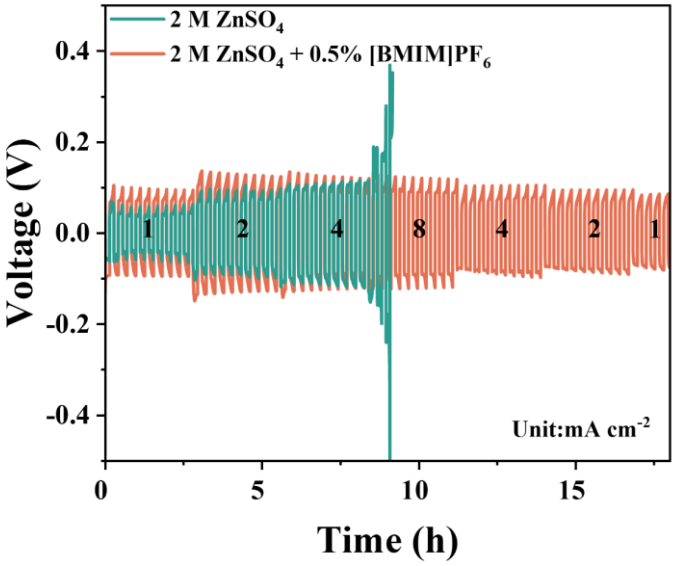

Fig. S14. Rate performance of Zn//Zn batteries in 2 M $ZnSO_4$+0.5% $[BMIM]PF_6$.

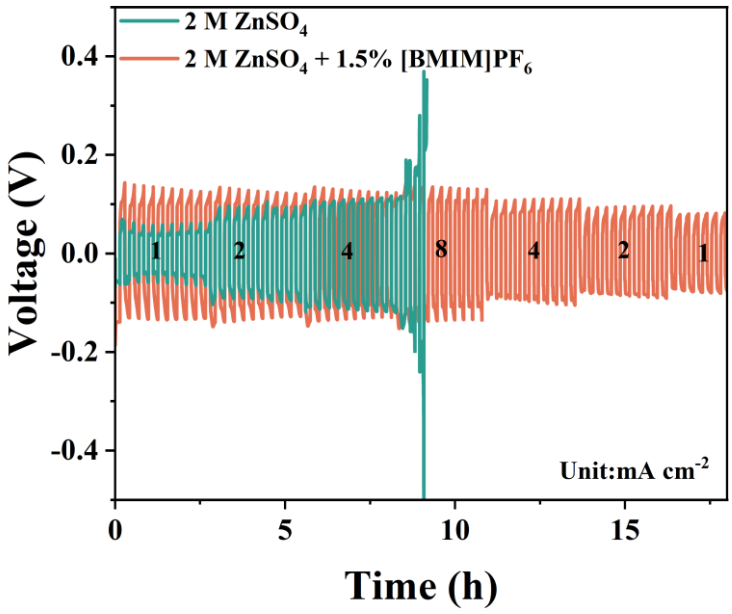

Fig. S15. Rate performance of Zn//Zn batteries in 2 M $ZnSO_4$+1.5% $[BMIM]PF_6$.

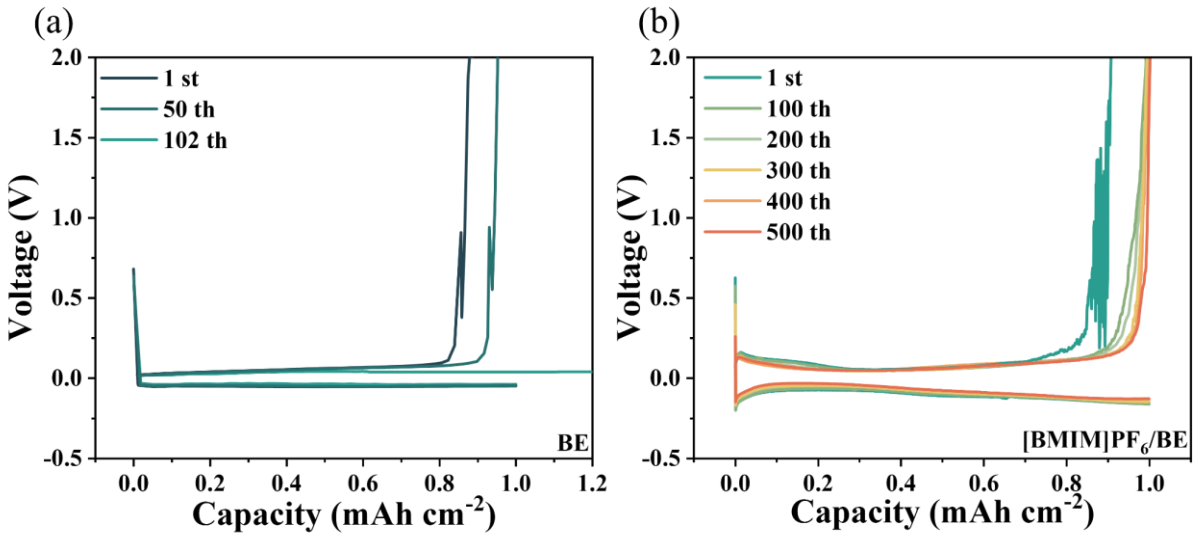

Fig. S16. corresponding voltage profiles at various cycles in $ZnSO_4$ electrolyte **(a)** without and **(b)** with [BMIM]PF_6 additive.

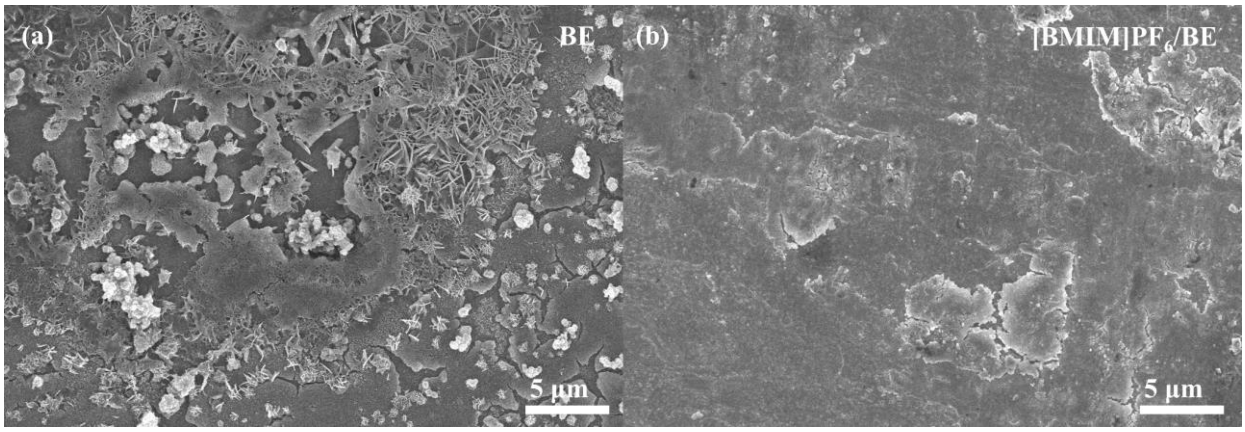

Fig. S17. SEM images of Zn anode surface morphology after cycling: **(a)** in BE system, **(b)** in [BMIM]PF_6/BE system.

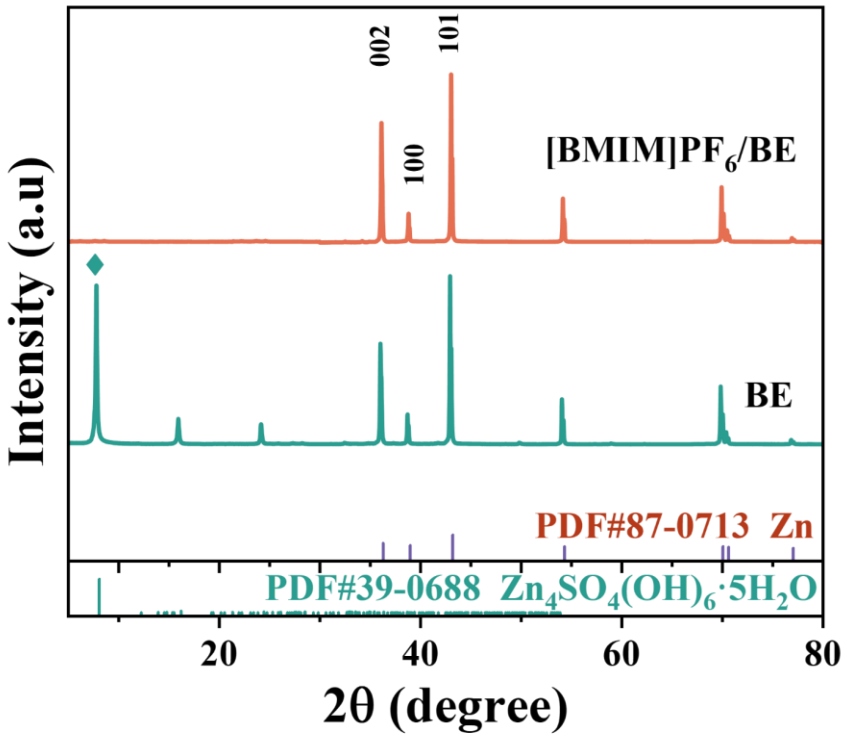

Fig. S18. XRD patterns of the Zn anodes with Zn//Cu half-cells in different electrolytes after 20 cycles at 1 mA cm^{-2} and 1 mAh cm^{-2}.

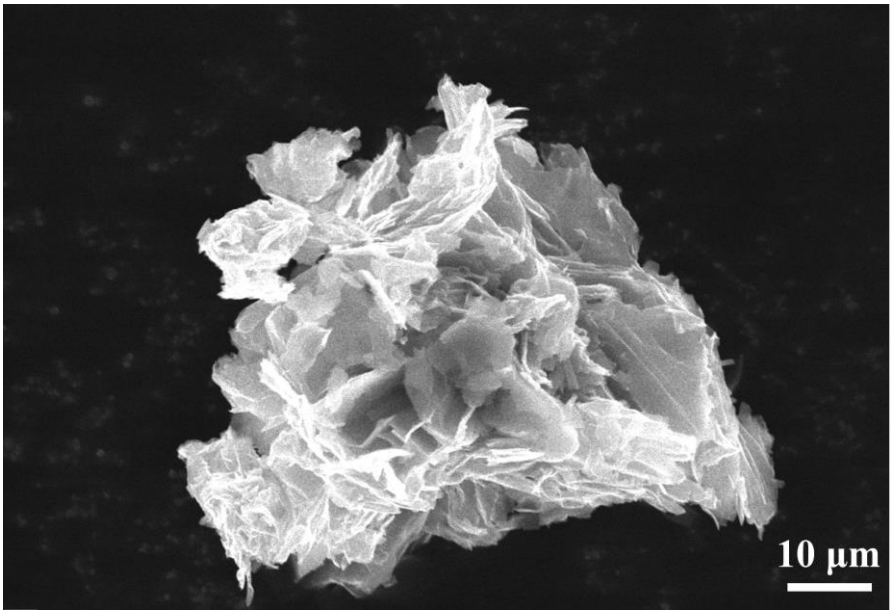

Fig. S19. SEM image of the $NH_4V_4O_{10}$ cathode material particle.

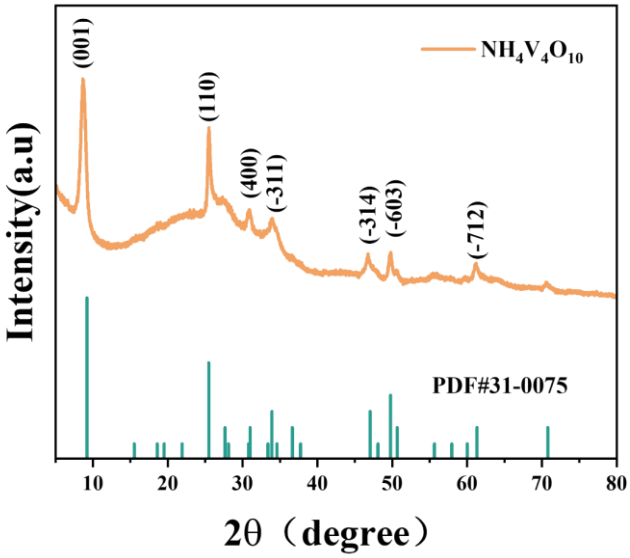

Fig. S20. XRD patterns of $NH_4V_4O_{10}$ powder.

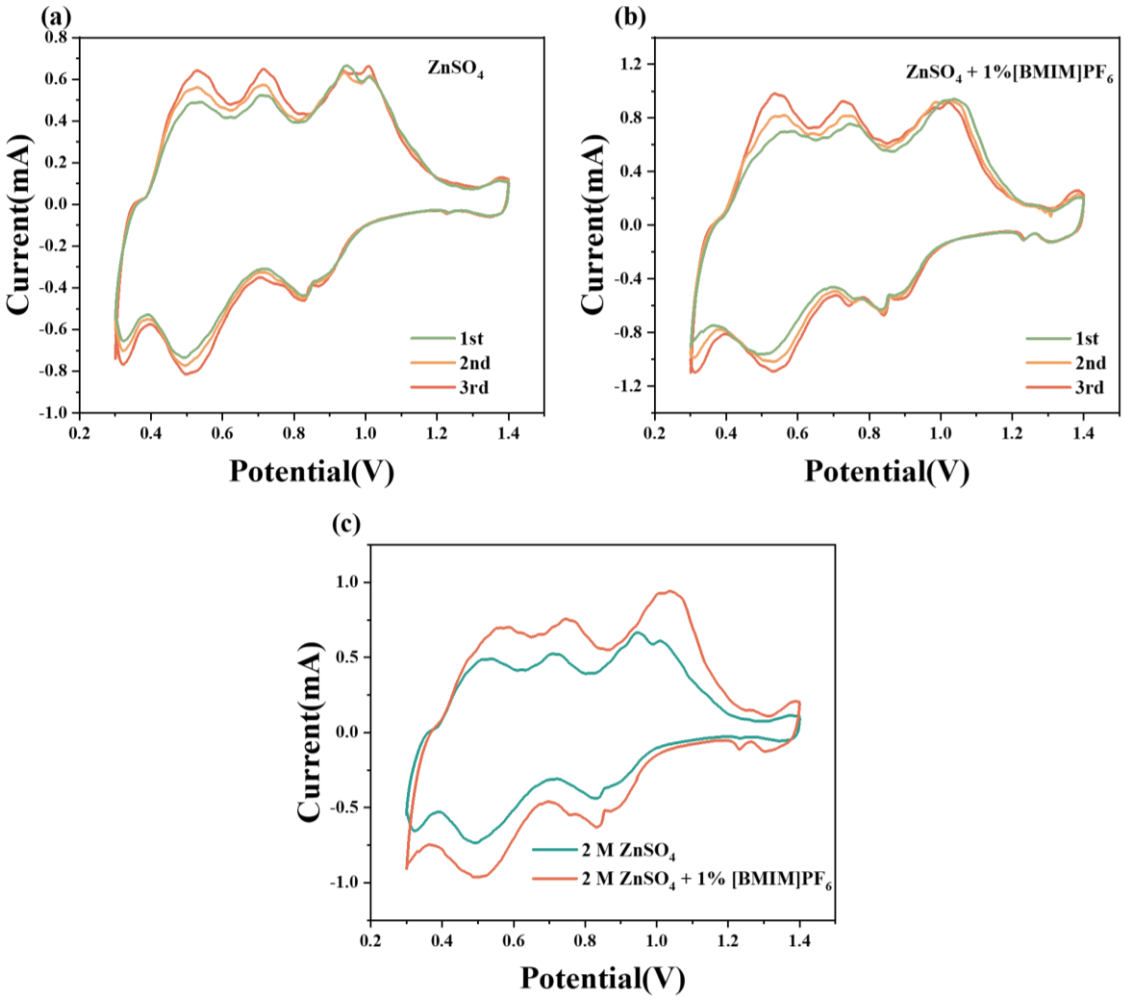

Fig. S21. CV profiles of the Zn//$NH_4V_4O_{10}$ batteries with different electrolytes. **(a)** Pure $ZnSO_4$ and **(b)** $ZnSO_4$+1% [BMIM]PF_6 electrolytes. **(c)** Comparison of the 3rd cycle of CV curves.

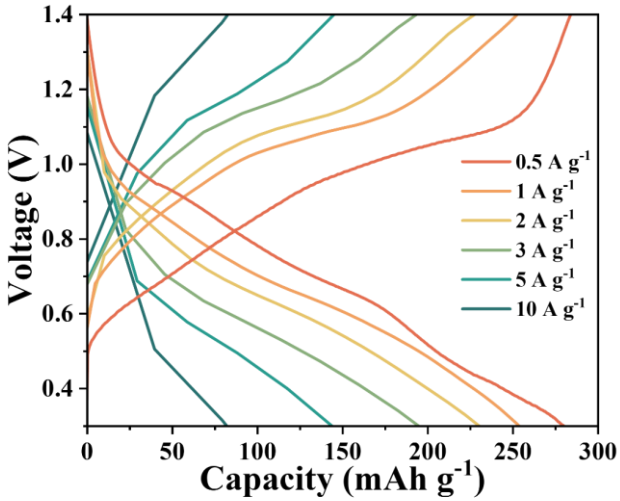

Fig. S22. Electrostatic charge/discharge curves of the Zn//$NH_4V_4O_{10}$ full cells at different current densities.

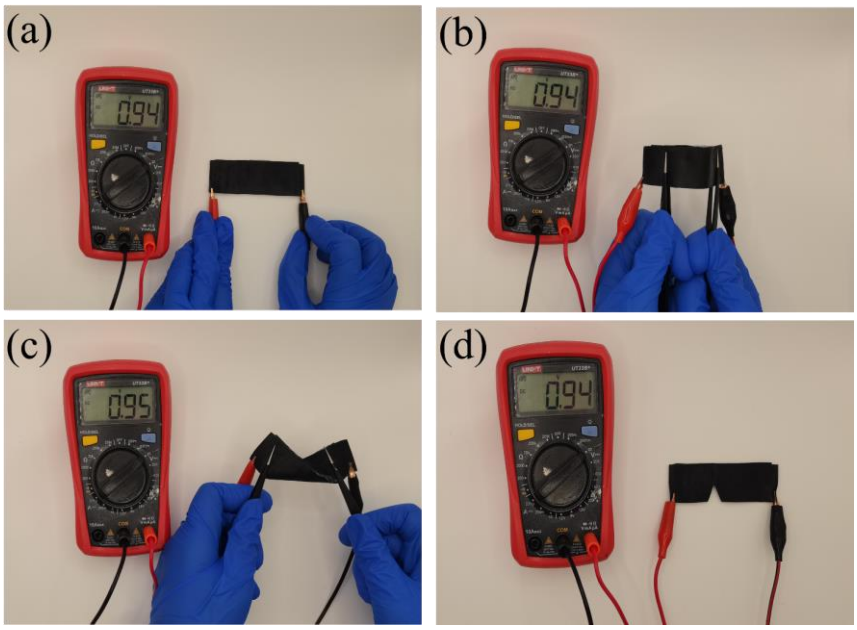

Fig. S23. Demonstrate the voltage variation of a PAM-[BMIM]PF_6 battery under **(a)** flat, **(b)** bent, **(c)** twisted, and **(d)** shear conditions.

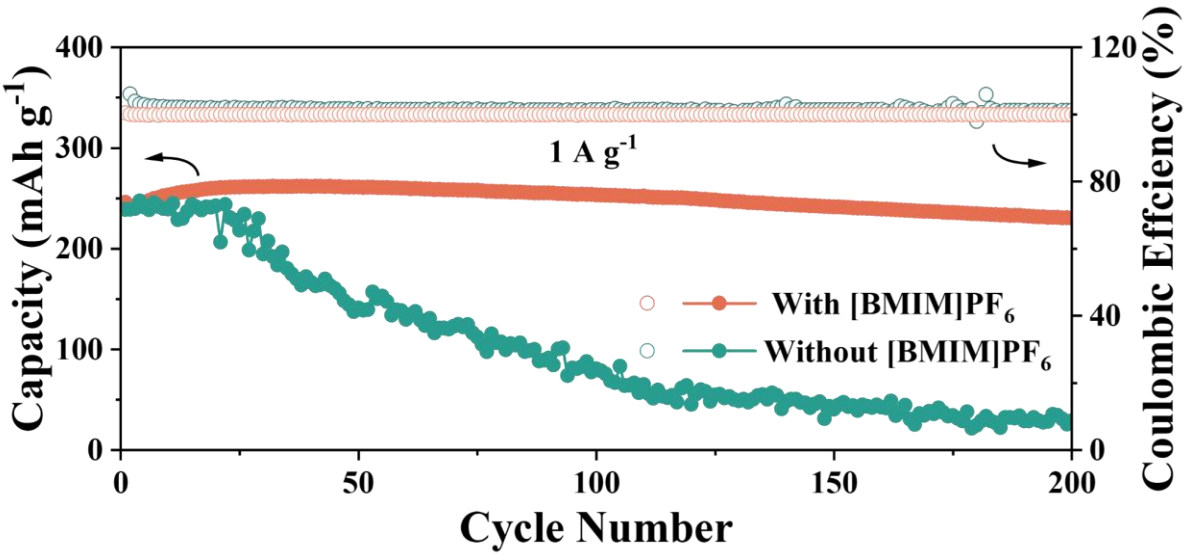

Fig. S24. Corresponding cycle performance of PAM-[BMIM]PF_6 flexible full cell at 1 A g^{-1}.

Table S1. Fitting parameters of Nyquist plots.

With $[BMIM]PF_6$			
T(K)	$R_{ct}(\Omega)$	Error (%)	$\ln(R_{ct}^{-1}/\Omega^{-1})$
303	1030.1	0.90	-6.94
313	885.4	0.83	-6.79
323	621.1	1.02	-6.43
333	344.3	1.07	-5.84
343	199.9	1.32	-5.29
Without $[BMIM]PF_6$			
T(K)	$R_{ct}(\Omega)$	Error (%)	$\ln(R_{ct}^{-1}/\Omega^{-1})$
303	469.6	1.56	-6.16
313	333.6	2.09	-5.81
323	199.9	2.15	-5.29
333	135.4	2.23	-4.91

The formula of the Arrhenius equation is expressed as follows:

$$\frac{1}{R_{ct}} = Aexp(-\frac{E_a}{RT})$$

where R_{ct} is the charge-transfer resistance, and A, T, R, and E_a represent the pre-exponential factor, absolute temperature, ideal gas constant, and activation energy, respectively.

Table S2. Fitting parameters of Nyquist plots.

With $[BMIM]PF_6$		
	R_S (Ω)	R_{ct} (Ω)
Pristine	1.42 / 1.44 / 1.46	409.19 / 471.17 / 495.32
10 th	1.58 / 1.59 / 1.54	55.49 / 62.95 / 74.47
20 th	1.75 / 1.77 / 1.82	24.65 / 32.39 / 57.14
30 th	1.63 /1.67 / 1.65	25.36 / 30.35 / 43.26
Without $[BMIM]PF_6$		
	R_S (Ω)	R_{ct} (Ω)
Pristine	1.49 / 1.52 / 1.50	1163.69 / 1181.13 / 1208.49
10 th	1.74 / 1.77 / 1.79	488.49 / 567.05 / 592.21
20 th	1.92 / 1.93 / 1.91	468.21 / 472.59 / 475.05
30 th	1.85 / 1.88 / 1.84	389.56 / 393.26 /396.34

Table S3. Performance comparison of symmetric Zn//Zn cells from the previously reported works involving electrolyte additives and our work.

No.	Electrolyte component	Current density/capacity (Zn//Zn)	Life (h)	Current density/capacity (Zn//Cu)	Coulombic efficiency (%)	Max cumulative capacity plated (Ah cm^{-2})	Ref
1	2 M $ZnSO_4$ + 0.08 M ZnF_2	1 mA cm^{-2}/1 mAh cm^{-2}	600	1 mA cm^{-2}/ 1 mAh cm^{-2}	99.6 (1000cycles)	3.2	[4]
2	1 M $ZnSO_4$ + 4 M EMImCL	1mA cm^{-2}/1 mAh cm^{-2}	500	1 mA cm^{-2}/ 1 mAh cm^{-2}	99.9 (90cycles)	0.25	[5]
3	2 M $ZnSO_4$ in glycerol/water (50/50)	1 mA cm^{-2}/1 mAh cm^{-2}, 2 mA cm^{-2}/6 mAh cm^{-2}	1500, 900	1 mA cm^{-2}/ 1 mAh cm^{-2}	98.3 (500cycles)	0.9	[6]
4	1 M $ZnSO_4$ + 75 mM Na_4EDTA	2 mA cm^{-2}/2 mAh cm^{-2}, 5 mA cm^{-2}/2 mAh cm^{-2}	450, 2000	0.5 mA cm^{-2}/ 0.5 mAh cm^{-2}	98.3 (300cycles)	5	[7]
5	1 M $ZnSO_4$ + 0.1 M $MgSO_4$	1mA cm^{-2}/0.25 mAh cm^{-2}	600	2 mA cm^{-2}/ 0.5 mAh cm^{-2}	expands to 400 h with about 100 C.E.	0.3	[8]
6	1 M $ZnSO_4$ + 0.01 M $Ce_2(SO_4)_3$	1 mA cm^{-2}/1 mAh cm^{-2}, 5 mA cm^{-2}/1 mAh cm^{-2}	400, 700	1 mA cm^{-2}/ 1 mAh cm^{-2}	97.0 (2000cycles)	1.75	[9]
7	2 M $ZnSO_4$ + 1 vol% DME	2 mA cm^{-2}/2 mAh cm^{-2}	380	1 mA cm^{-2}/ 0.4 mAh cm^{-2}	99.1 (200cycles)	0.38	[10]
8	2 M $ZnSO_4$ + 0.05mg mL^{-1} $Ti_3C_2T_x$	2 mA cm^{-2}/1 mAh cm^{-2}, 4 mA cm^{-2}/5 mAh cm^{-2}	1180, 250	1 mA cm^{-2}/ 1 mAh cm^{-2}	98.6 (100cycles)	1.18	[11]
9	2 M $ZnSO_4$ + 0.5 g L^{-1} TMBAC	2 mA cm^{-2}/2 mAh cm^{-2}, 10 mA cm^{-2}/5 mAh cm^{-2}	900, 470	0.5 mA cm^{-2}/ 1 mAh cm^{-2}	99.0 (200cycles)	2.35	[12]
10	7.6 mM $ZnCl_2$+ 0.05 mM $SnCl_2$	3 mA cm^{-2}/3 mAh cm^{-2}	500	0.5 mA cm^{-2}/ 0.5 mAh cm^{-2}	99.7 (200cycles)	0.75	[13]
11	4 M $Zn(TFSI)_2$ + 4 M $P_{444(2O1)}$-TFSI	0.5 mA cm^{-2}/0.5 mAh cm^{-2}, 1 mA cm^{-2}/1 mAh cm^{-2}, 2.5 mA cm^{-2}/2.5 mAh cm^{-2}	6000, 800, 280	0.5 mA cm^{-2}/ 5 mAh cm^{-2}	>99 (16cycles)	1.5	[14]
12	1 M $Zn(TFSI)_2$ + 0.25 M Ace	1 mA cm^{-2}/0.5 mAh cm^{-2}	100	0.5 mA cm^{-2}/ 0.5 mAh cm^{-2}	98 (10cycles)	1	[15]
13	1 M $ZnSO_4$ +0.25PA	5 mA cm^{-2}/1 mAh cm^{-2}	400	/	/	/	[16]
14	1 M $ZnSO_4$ +10%TG	2 mA cm^{-2}/0.67 mAh cm^{-2}	670	2 mA cm^{-2}/ 1 mAh cm^{-2}	99.49 (300cycles)	/	[17]
This work	2 M $ZnSO_4$ + 1 % $[BMIM]PF_6$	1 mA cm^{-2}/1 mAh cm^{-2}, 4 mA cm^{-2}/0.5 mAh cm^{-2}, 4 mA cm^{-2}/4 mAh cm^{-2}	800, 1000, 400	1 mA cm^{-2}/ 1 mAh cm^{-2}	99.7 (500cycles)	2.31	This work

3. References

1. H. Sun, J. Phys. Chem. B, 1998, **102**, 7338-7364.
2. H. Sun, P. Ren, J.R. Fried, Comput. Theor. Polym. Sci., 1998, **8**, 229-246.
3. O. Borodin, M. Olguin, P. Ganesh, P.R.C. Kent, J.L. Allen, W.A. Henderson, Phys. Chem. Chem. Phys., 2016, **18**, 164-175.
4. Y. An, Y. Tian, K. Zhang, Y. Liu, C. Liu, S. Xiong, J. Feng, Y. Qian, Adv. Funct. Mater., 2021, **31**, 2101886.
5. Q. Zhang, Y. Ma, Y. Lu, L. Li, F. Wan, K. Zhang, J. Chen, Nat. Commun., 2020, **11**, 4463.
6. Y. Zhang, M. Zhu, K. Wu, F. Yu, G. Wang, G. Xu, M. Wu, H.-K. Liu, S.-X. Dou, C. Wu, J. Mater. Chem. A, 2021, **9**, 4253-4261.
7. S.-J. Zhang, J. Hao, D. Luo, P.-F. Zhang, B. Zhang, K. Davey, Z. Lin, S.-Z. Qiao, Adv. Energy Mater., 2021, **11**, 2102010.
8. P. Wang, X. Xie, Z. Xing, X. Chen, G. Fang, B. Lu, J. Zhou, S. Liang, H.J. Fan, Adv. Energy Mater., 2021, **11**, 2101158.
9. K.A. Owusu, X. Pan, R. Yu, L. Qu, Z. Liu, Z. Wang, M. Tahir, W.A. Haider, L. Zhou, L. Mai, Mater. Today Energy, 2020, **18**, 100529.
10. H. Huang, D. Xie, J. Zhao, P. Rao, W.M. Choi, K. Davey, J. Mao, Adv. Energy Mater., 2022, **12**, 2202419.
11. J. Cao, D. Zhang, C. Gu, X. Wang, S. Wang, X. Zhang, J. Qin, Z.-S. Wu, Adv. Energy Mater., 2021, **11**, 2101299.
12. K. Guan, L. Tao, R. Yang, H. Zhang, N. Wang, H. Wan, J. Cui, J. Zhang, H. Wang, H. Wang, Adv. Energy Mater., 2022, **12**, 2103557.
13. L. Cao, D. Li, F.A. Soto, V. Ponce, B. Zhang, L. Ma, T. Deng, J.M. Seminario, E. Hu, X.-Q. Yang, P.B. Balbuena, C. Wang, Angew. Chem. Int. Ed., 2021, **60**, 18845-18851.
14. L. Ma, T.P. Pollard, Y. Zhang, M.A. Schroeder, M.S. Ding, A.V. Cresce, R. Sun, D.R. Baker, B.A. Helms, E.J. Maginn, C. Wang, O. Borodin, K. Xu, Angew. Chem. Int. Ed., 2021, **60**, 12438-12445.
15. H. Qiu, X. Du, J. Zhao, Y. Wang, J. Ju, Z. Chen, Z. Hu, D. Yan, X. Zhou, G. Cui, Nat. Commun., 2019, **10**.

16. Y. Chen, F. Gong, W. Deng, H. Zhang, X. Wang, Energy Storage Mater., 2023, **58**, 20-29.

17. Z. Liu, R. Wang, Q. Ma, J. Wan, S. Zhang, L. Zhang, H. Li, Q. Luo, J. Wu, T. Zhou, J. Mao, L. Zhang, C. Zhang, Z. Guo, Adv. Funct. Mater., 2024, **34**, 2214538.